Photo-Stable Organic Thin-Film Transistor Utilizing a New Indolocarbazole Derivative for Image Pixel and Logic Applications

*Ji Hoon Park, Hee Sung Lee, Soohyung Park, Sung-Wook Min, Yeonjin Yi, Cheon-Gyu Cho, Jiwon Han, Tae Woong Kim, and Seongil Im**

Small molecule pentacene layer has been a representative among many organic thin-film transistor (OTFT) channels with decent p-type mobilities, but it is certainly light-sensitive due to its relatively small highest occupied molecular orbital-lowest unoccupied molecular orbital (HOMO-LUMO) gap (1.85 eV). Although a few other small molecule-based layers have been reported later, their photo-stabilities or related device applications have hardly been addressed. Here, a new photostable organic layer is reported, heptazole ($C_{26}H_{16}N_2$), which has almost the same HOMO level as that of pentacene but with a higher HOMO-LUMO gap (≈2.95 eV). This heptazole OTFT displays a decent mobility comparable to that of conventional amorphous Si TFTs, showing good photostability unlike pentacene OTFTs. An image pixel driving the photostable heptazole OTFT connected to a pentacene/Al Schottky photodiode is demonstrated. This heptazole OTFT also conveniently forms a logic inverter coupled with a pentacene OTFT, sharing Au for source/drain.

1. Introduction

Small molecule pentacene has attracted much attention from researchers in its solid crystalline thin-film form for the last decade, since the organic pentacene thin-film shows decent *p*-channel mobilities (0.1–5 $cm^2 V^{-1} s^{-1}$) and reasonable ambient stabilities as an organic semiconductor.[1] Using pentacene films as an active charge transport layer, organic thin-film transistors (OTFTs) were developed to provide such a variety of functional devices as display drivers, logic inverters, ring oscillators, and even image pixels.[2] But they were certainly in lack of photostability, which originates from their relatively small bandgap and interfacial trap located at semiconductor/dielectric interface in TFT structure.[3] Following pentacene, other *p*-type small molecules were thus fabricated, to circumvent some remaining drawbacks of pentacene. Indolo[3,2-*b*]carbazole, [1]benzothieno[3,2-b]benzothiophene (BTBT), and dinaphtho-[2,3-b:20,30-f]thieno[3,2-b] thiophene(BTBT) are the exemplary new *p*-type molecules which were respectively reported by Wu et al., Yamamoto and Takimiya, and Ebata et al.[4] According to their results, the highest occupied molecular orbital-lowest unoccupied molecular orbital (HOMO-LUMO) gap of indolo[3,2-*b*]carbazole and DNTT layers are respectively 2.8 and 3.0 eV, which are quite higher than that of pentacene (1.85 eV), so that the newly developed small molecule-based layers might be more photostable than old pentacene layer in OTFT applications. However, the photostability of such organic transport layers has hardly been addressed yet and no related applications have been reported, either.[4] In the present work, we synthesized another indolocarbazole-type small molecule, 8,16-dihydrobenzo[a]benzo[6,7]indolo[2,3-*h*]carbazole (heptazole: $C_{26}H_{16}N_2$) which has almost the same HOMO level as that of pentacene but with higher HOMO-LUMO gap of ≈2.95 eV, to fabricate a small molecule-based OTFT. This molecule has a rigid, linear, and coplanar conjugated structure along with a extended π-orbital area in the aromatic core comparing to pentacene. The field-effect mobility of our new OTFT turns out to be ≈0.21 $cm^2 V^{-1} s^{-1}$, which is lower than that of the pentacene OTFT on the same dielectric layer. However, it certainly displays good photostability under visible illuminations unlike pentacene devices. Taking advantages of such photostabilities, we fabricated an image sensor pixel where our photostable heptazole-based OTFT and photo-detecting pentacene Schottky diode are coupled. Besides the photostability benefit, the heptazole-based OTFT gained another benefit when connected to pentacene-based OTFT, conveniently forming a logic inverter where the two OTFTs use an identical source/drain electrode Au in common while they have different threshold voltages each other.

Dr. J. H. Park, H. S. Lee, S. Y. Park, S.-W. Min, Prof. Y. Yi, Prof. S. Im
Institute of Physics and Applied Physics
Yonsei University
Seoul, 120-749, Republic of Korea
E-mail: semicon@yonsei.ac.kr
Prof. C.-G. Cho
Department of Chemistry
Hanyang University
17 Haengdang-Dong, Sungdong-Ku, Seoul, 133-791, Korea
Dr. J. Han, Dr. T. W. Kim
Samsung Display Co., Ltd
#95, Samsung 2-ro, Giheung-gu, Yongin-si, Gyeonggi-do 446-711, Korea

DOI: 10.1002/adfm.201301783

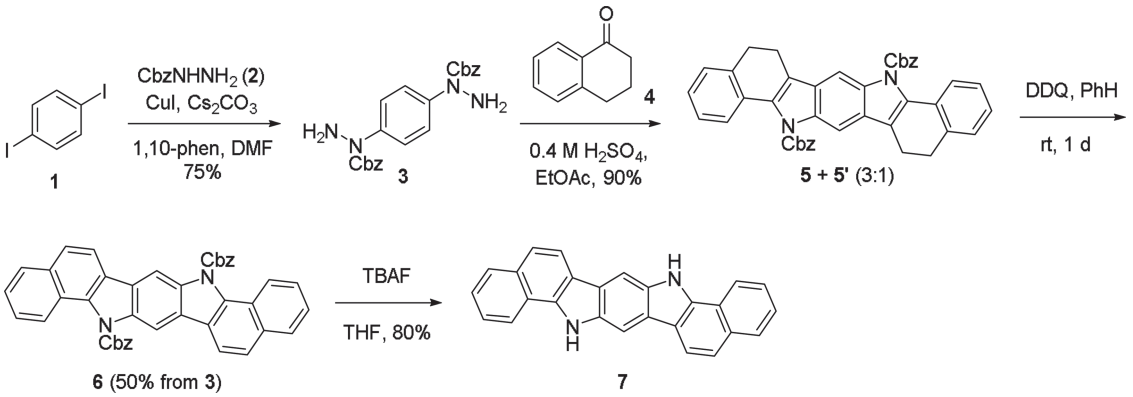

Scheme 1. Synthesis of 8,16-dihydrobenzo[*a*]benzo[6,7]indolo[2,3-*h*]carbazole (heptazole)

2. Results and Discussion

2.1. Characterization of Heptazole Thin-Film

The brief scheme for synthesis of heptazole and molecule structure are shown in **Scheme 1** and **Figure 1**a, respectively. In order to achieve some fundamental understandings on our newly synthesized heptazole semiconductor film, X-ray diffraction (XRD) and atomic force microscopy (AFM) measurements were implemented on 50 nm-thick heptazole films along with the identically-thick pentacene, which would be a reference to be compared. According to Figure 1b, strong XRD peaks of heptazole thin-film (deposited on p^+-Si substrate) are located at $2\theta = 5.06°$ and 10.12°, to respectively indicate d spacings of 17.44 Å and 8.73 Å from (001) and (002) reflections, as an evidence of descent crystalline ordering, which would provide the potential for an active charge transport layer. For comparison, the XRD result of pentacene film deposited on the identical substrate shows similarly-intense but stronger reflections at d spacings of 15.22 Å ($2\theta = 5.80°$, (001)) and 7.66 Å ($2\theta = 11.54°$, (002)), which are very similar to those reported elsewhere.[5] Moreover, pentacene film does show more clear (003) and

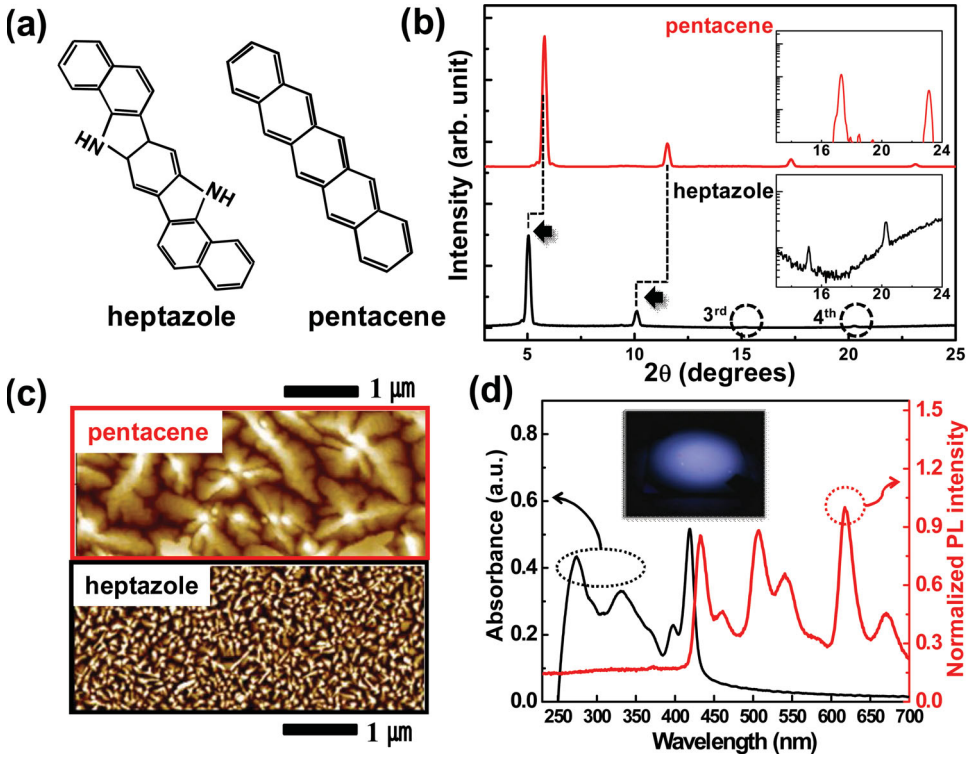

Figure 1. a) Chemical structure of heptazole and pentacene molecules utilized as semiconductor layer in this study. b) X-ray diffraction results from our pentacene and heptazole thin-film grown on Si substrate. The inset XRD data present (003) and (004) reflections from pentacene and heptazole thin-films in log scale intensity. The crystalline quality of solid pentacene appears superior to that of heptazole. c) AFM images of pentacene and heptazole thin-films grown on spin-coated CYTOP/Si. d) UV-visible absorption (black) and photoluminescence (red) spectra of heptazole thin-films. Inset shows PL image obtained from our heptazole thin-film, displaying a weak white emission under a UV excitation of 0.3 mW.

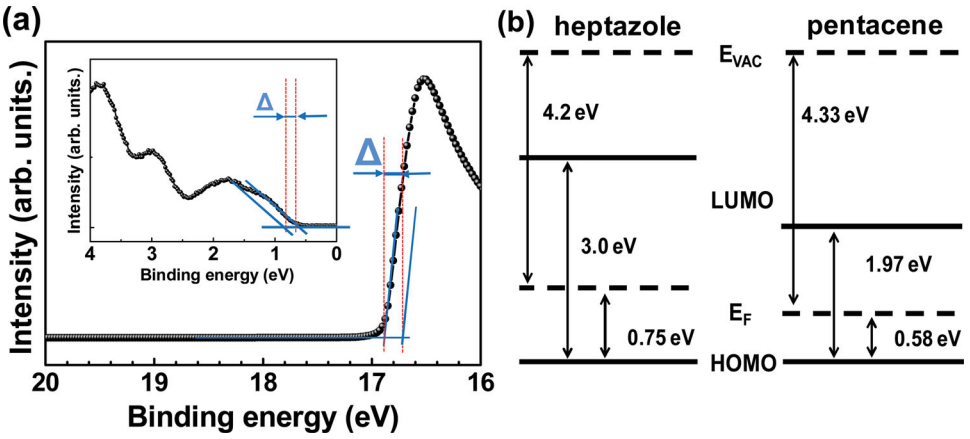

Figure 2. Measured He I (21.22 eV) UPS spectra of ultra-thin heptazole film (10 nm) on ITO/glass substrate considering thermal and instrumental broadening (0.1 eV). a) Normalized secondary electron cut-off region and inset shows HOMO onset with the removal of background. b) UPS-defined energy level diagrams of heptazole (left) and pentacene (right) layers deposited on indium-tin-oxide (ITO)/glass.

(004) reflections which were hardly seen from heptazole film in linear scale intensity but only identified by log scale (insets of Figure 1b). We thus regard that the heptazole film is less ordered than pentacene one while its d spacing is longer than that of crystalline pentacene due to the length of its single molecule or due to molecule's standing angle with respect to the substrate. Crystallography and synthesis studies of heptazole-series bearing various pendant N-alkyl groups are reported by our co-workers,[6] and here we introduce the synthesis and molecular structure of single heptazole molecule without the alkyl chain in the inset of Scheme 1 and Figure 1a, respectively. In Figure 1c, AFM images of 50 nm-thin pentacene and heptazole films deposited on CYTOPs are displayed; both have quite similar granular morphologies but much larger grains are obviously observed from pentacene as another evidence of inferior crystallinity of heptazole layer. Figure 1d displays the optical absorption and photoluminescence (PL) spectra of heptazole thin-film as deposited on corning glass and p^+ -Si, respectively. Two characteristics are observed here from the layer: its large HOMO-LUMO gap and white light emission (spectrally mixed with red, green, and blue lights of 438, 506, 617 nm) which is displayed in the inset and was visible by raw eyes under 345 nm ultraviolet (UV) excitation of 0.3 mW. Such quite a strong PL emission is different from the weak PL results previously reported with crystalline pentacene, indicating that our crystalline heptazole is probably less ordered than the solid pentacene in general (as evidenced by XRD and AFM data).[7] More important is probably the HOMO-LUMO gap which is as large as 2.95 eV (from 420 nm absorption peak), since this property may result in organic devices which are stable under visible illuminations.

We also carried out UV photoemission spectroscopy (UPS) measurements with a ≈10 nm-thin heptazole film that was thermally-evaporated on indium-tin-oxide (ITO)/glass substrate, since this information is one of the essentials for metal/organic contact. The UPS spectra were obtained with a sample bias of –15 V in normal emission geometry to measure the secondary electron cut-off. The way how we determine thermal and instrumental broadening (≡ total broadening, say Δ) of UPS spectra is described elsewhere.[8] The work function of heptazole layer is determined to be 4.2 eV after taking the broadening Δ (0.1 eV) and secondary electron cut-off (SEC) position into account as shown in **Figure 2**a. Then, the HOMO position of heptazole is seen at 0.75 eV below the Fermi level as shown in inset of Figure 2a after considering the Δ, too. As illustrated in the energy diagram, the HOMO level of our heptazole appeared to be ≈4.95 eV which is interestingly similar to that of pentacene, although its Fermi-level (E_F) was located at ≈0.75 eV above HOMO while that of pentacene is to be at 0.58 eV above HOMO; then a higher hole carrier density would be expected from pentacene.[9]

2.2. Photostability Characterizations and PECCS Analysis on the Heptazole OTFT

The photostability of heptazole film is observed from the photo-induced transfer curves (drain current-gate voltage; I_D–V_G) as obtained from our heptazole-based OTFT at a drain voltage (V_D) under a linear regime (V_D = –0.5 V). A schematic cross-section of our test device is illustrated in the inset, along with a brief view of photoexcited charge collection spectroscopy (PECCS) setup to analyze the interfacial trap density-of-states (trap DOS) and HOMO-LUMO gap. According to **Figure 3**a, the heptazole-based OTFT appears very photostable showing negligible photo- induced threshold voltage (V_{th}) shift toward (+) direction with visible red (600 nm), green (555 nm), and blue (475 nm) monochromatic illuminations, even though the OTFT seriously reacts with 355 nm UV showing more than +15 V shift. Such a small photo-response under visible illuminations not only indicates that our heptazole active layer has a higher HOMO-LUMO gap than blue spectral energy, but also indicates that only a small density of effective trap charges (Q_{eff}) exists at the heptazole channel/CYTOP dielectric interface of the OTFT. These photo-responses were more systematically analyzed by PECCS measurements and the detailed information is displayed in Figure 3b, according to which the photo-induced ΔQ_{eff} and interfacial trap DOS risings start at ≈2.95 eV and

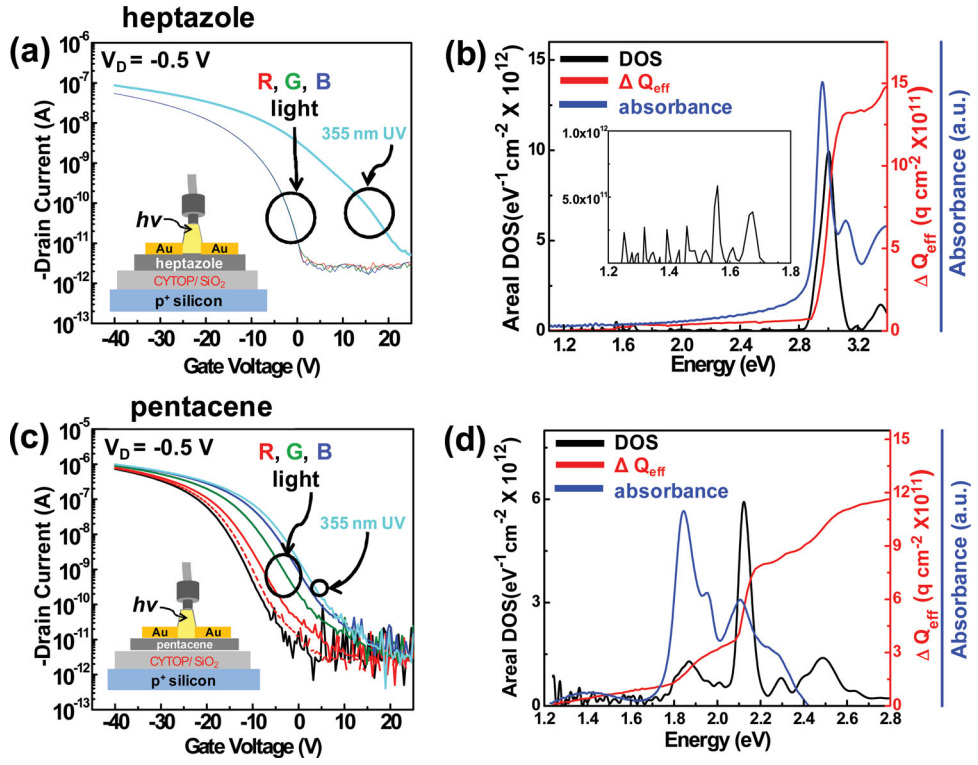

Figure 3. a) Photo-induced transfer curves of heptazole-TFT under red (600 nm), green (555 nm), blue (475 nm) and 355nm UV monochromatic light. Inset shows schematic view of heptazole-TFT under monochromatic lights that were used for PECCS measurements. b) PECCS-induced DOS plot (black) for heptazole-TFT as obtained by differentiating ΔQ_{eff} (ε) curve (red) with photon energy, ε. The optical absorbance spectrum (blue) of heptazole film is overlaid on DOS and ΔQ_{eff} (ε) plots for comparison. The inset DOS plot shows the densities of traps which are located at the heptazole/CYTOP interface appearing negligible. c) Photo-induced transfer curves of pentacene-TFT under identical monochromatic light used in (a). The red-dashed line represents transfer characteristic under red (695nm) light, which is below HOMO-LUMO gap energy. d) PECCS-utilized DOS plots (black) of pentacene OTFT fabricated with CYTOP/SiO_2/p^+ silicon. Photon flux for PECCS was at least 5×10^{14} cm^{-2} s^{-1} (optical power density, 0.2 mW cm^{-2}).

the trap DOS profile makes its peak at 3.0 eV while the optical absorption spectra of 50 nm-thick heptazole film (on glass) are overlapped as a reference with respect to the trap DOS and ΔQ_{eff} profiles.[10] The HOMO-LUMO gap is thus regarded to be ≈3.0 eV, which is very consistent with the value (2.95 eV) from optical absorption. The 0.05 eV difference may be due to excition binding energy in crystalline heptazole, and we regard that 3 eV is large enough for an organic device to circumvent the device instability due to visible range illuminations. Actual interface trap DOS appears to be minimal and located much below 3 eV, and for detail information the data were zoomed in as shown in the inset where the small trap DOS peaks are observed near 1.55 and 1.65 eV. The trap DOS peak intensity is as small as 6.1×10^{11} q cm^{-2} eV^{-1} (where q is quantity of electric charge, -1.6×10^{19} C) which is two orders of magnitude smaller than that of the HOMO-LUMO peak, resulting in little photo-response under the visible illuminations. In contrast, in Figure 3c, the photo-response from pentacene OTFT fabricated on the same CYTOP/SiO_2/p^+-Si substrate was significant under visible illuminations. According to the PECCS and optical absorption spectra of Figure 3d, pentacene OTFT begins to show its noticeable photo-response near 1.85 eV which is regarded as the first HOMO-LUMO gap of solid pentacene. [3b,c,d] The interfacial trap density in pentacene OTFT is ≈1.7×10^{11} cm^{-2} (= $\Delta Q_{eff}/q$) at 1.8 eV, which is a few times higher than that of heptazole OTFT (≈7×10^{10} cm^{-2}) at the HOMO-LUMO gap of heptazole, 2.95 eV. Therefore, it is certainly acknowledged that our new heptazole channel layer on CYTOP dielectric results in little photo-response under the visible range of illuminations.

2.3. Organic Image-Pixel Composed of Heptazole OTFT and Pentacene/Al Schottky Photodiode

Based on the photoelectric characteristics of crystalline heptazole and pentacene, we fabricate an image pixel for our first device application. The image pixel was composed of a Schottky diode with 150 nm-thick pentacene and an OTFT with 60 nm-thin heptazole, which was thermally evaporated on the gate (G) dielectric of CYTOP/thin Al_2O_3 double layer. A 200 nm-thick Au was deposited on heptazole as the top contact source/drain (S/D) electrode, while semitransparent conductive NiO_x and Al were respectively deposited as the cathode and anode of pentacene Schottky diode. **Figure 4**a,b display the schematic illustration and optical microscopy image of our pixel, respectively. (Also see Figure S1, Supporting Information for schematic top and cross-section views.) Our pixels appear opaque and dark particularly in Schottky diode area because the pentacene in the diode is too thick (150 nm) on opaque Al, although the OTFT

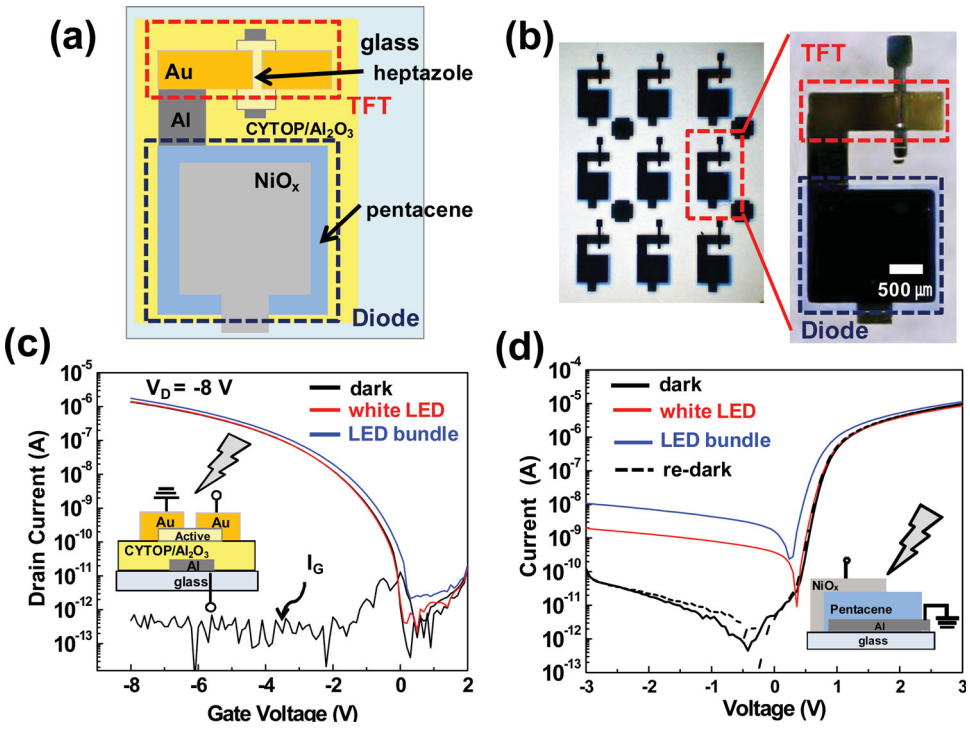

Figure 4. a) Schematic top-view of the image pixel composed of heptazole-TFT and pentacene/Al Schottky diode. b) Photograph of the image pixel array (left) and magnified image of one pixel (right). c) Dark and photo-induced transfer characteristics of heptazole OTFT. d) Dark and photo I-V curves of pentacene/Al Schottky diode. Optical power densities were ≈50 μW cm^{-2} and ≈1.2 mW cm^{-2} for white LED and its bundle, respectively.

region shows a little contrast in a magnified view. Prior to pixel operation, we initially measured static response of each device under commercial white light emitting diode (LED) and LED bundle; Figure 4c,d display the respective *I–V* curves of the heptazole-OTFT and pentacene diode, obtained under a white LED and a LED bundle (containing over ≈30 individual white LEDs). The photoelectric response of heptazole TFT appears insignificant under intense white LED (≈50 μW cm^{-2}) and only a little photoelectric reaction was observed under an intense white LED bundle (≈1.2 mW cm^{-2}). On the contrary, significant photoelectric effect is observed from our 150 nm-thick pentacene/Al Schottky diode under the both white LED and LED bundle lamp, including off-current increase, which reduces the on/off ratio of our diode from the initial ≈5 × 10^5 to less than ~10^4 (for white LED case) or to ~10^3 (for the LED bundle).

Combining these two devices in series (by connecting drain electrode of heptazole-TFT and cathode of pentacene/Al Schottky diode with Au; also see the inset circuit of **Figure 5**a), we could fabricate an image pixel, to measure V_{OUT} signal with respect to input voltage (V_{IN}) under dark and a white LED, that illuminates both of TFT and diode (Figure 5a; supply voltage, V_{DD} = −3 V). The plots of Figure 5a are thus a sort of voltage transfer characteristic (VTC) curves that could be obtained with or without white light LED, and here we selected two V_{IN} voltages of –0.3 V and 0.1 V (as indicated by two vertical lines), to obtain a time-domain ON/OFF pixel behavior. Figure 5b shows the time-domain pixel behavior, which appears consistent with the results of Figure 5a in the aspects of V_{OUT} level although few seconds of time delay was also shown due to too low supply current (I_{DD}) we used. This means that the channel resistance is presently high enough to cause long RC time delay, but pixel speed will be improved by choosing a large V_{IN} after enlarging the size of the Schottky diode, to eventually reduce the channel resistance. (Pixel size engineering is necessary for an optimal device performance.) The pixel response upon the illumination intensity of the white LED was characterized as another important device property under –1.2 V of V_{DD} in VTC curves of Figure 5c, for which the intensity of white LED was simply adjusted by the length variation between image pixel and white LED; three different LED intensities (60, 50, and 10 μW cm^{-2}, in order) but with the same spectra are accordingly plotted in the inset. For the time-domain pixel behavior under different light intensities, we used a V_{IN} of 0.2 V that might optimally present the dynamic photo-response (Figure 5d), and the dynamic results were apparently consistent with the static VTC curves of Figure 5c in terms of V_{OUT} level.

2.4. Heptazole-Pentacene Coupled Depletion-Load Inverter

For our second device application, we fabricated depletion-load type inverters, connecting two *p*-channel TFTs with heptazole and pentacene in series.[11] Our depletion-load type inverter is shown in the photograph image of **Figure 6**a, where the left- and right-side TFTs are load and driver, respectively. Here, Au was commonly used for the source/drain electrodes of both devices since pentacene and heptazole have almost an identical HOMO level each other, while Al was used as gate for both devices. According to Figure 6b, respective transfer curves of pentacene and heptazole TFTs with the same W/L ratio (500/90 μm)

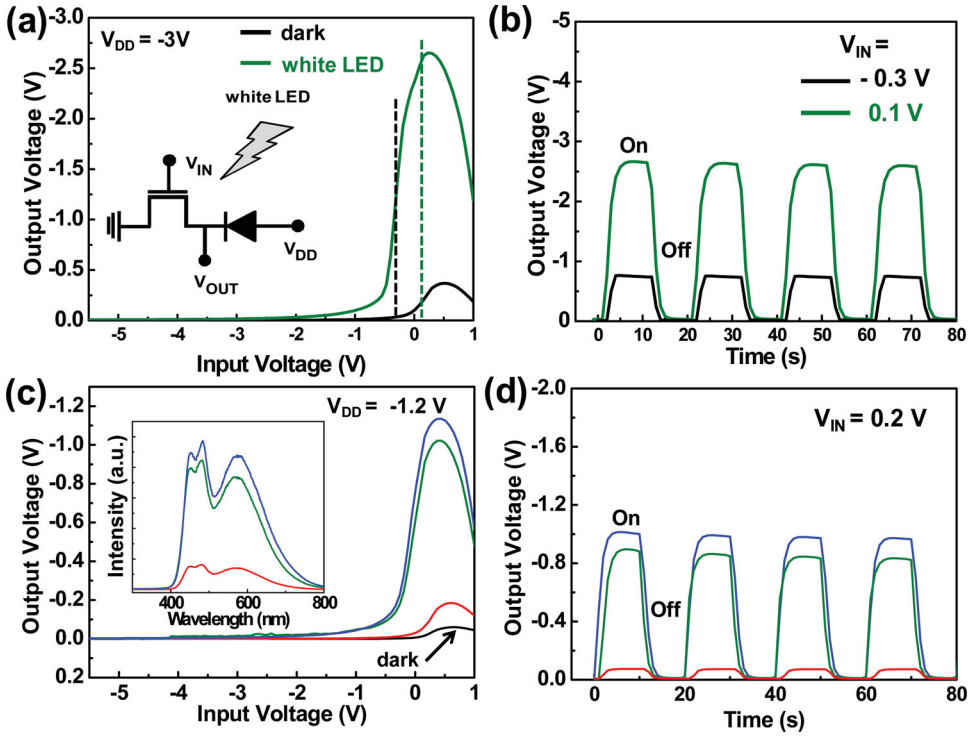

Figure 5. a) Voltage transfer characteristic (VTC) curve of our image pixel under dark (black line) and white LED light (green line). Two vertical dash lines indicate two V_{IN}s we used. b) Time domain output signals were thus measured at the two respective V_{IN}s under white LED blinking (on and off). c) VTC curves of our image pixel under dark (black line) and intensity-adjusted white LED. Inset shows the LED spectra with different intensities: 60, 50, and 10 μW cm^{-2}, in order. d) Time domain output voltage signals achieved under the different intensities of white LED.

display the different threshold voltages (V_{th}) of –2 and 0 V while the on-current of pentacene OTFT appears higher than that of heptazole-based device. Based on the individual transfer curve characteristics, the pentacene-channel TFT becomes the driver of our inverter, since a transistor with a larger V_{th} plays as a driver in general. Our heptazole-channel TFT shows lower satu-

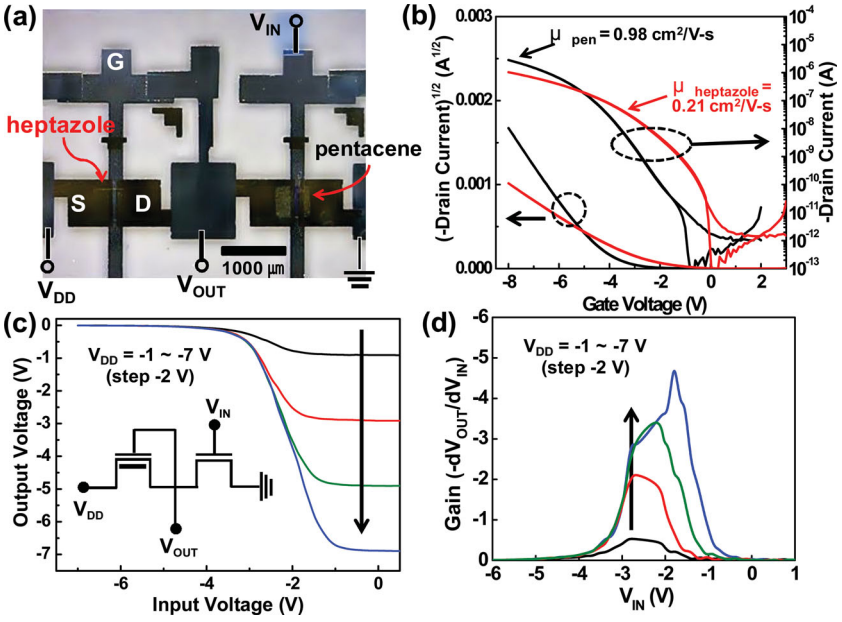

Figure 6. a) Photographic image of our inverter. Two types of OTFTs are interconnected with Al. b) Transfer curve characteristics of heptazole-TFT (red) and pentacene-TFT (black). These two OTFTs show different threshold voltages. c) Voltage transfer curve (VTC) characteristics and schematic circuit (inset) of our inverter composed of heptazole-TFT (load) and pentacene TFT (driver). d) Voltage gain plot derived from the VTC curves.

ration mobility (0.21 $cm^2 V^{-1} s^{-1}$) than that (0.98 $cm^2 V^{-1} s^{-1}$) of pentacene-based one, however its sub-threshold swing (S.S.) appears superior. These results of smaller V_{th} and S.S. are understandable if we re-examine the interfacial trap DOS and ΔQ_{eff} in Figure 3b,d, where the interface trap DOS of heptazole and pentacene TFTs are respectively measured and the interfacial Q_{eff} of heptazole TFT appears rather smaller. On one hand, it is not surprising that the mobility of pentacene TFT is higher than that of heptazole device, since the crystalline quality of heptazole film is regarded inferior to that of pentacene as respectively shown in XRD and AFM data of Figure 1b,c. Corresponding output characteristics from heptazole and pentacene OTFTs are also provided in Figure S2, Supporting Information. Smaller I_D current of heptazole device is observed but with the same Ohmic behavior as that of pentacene device at the initial V_D stage, indicating that both organic channels have similarly good Ohmic contacts with Au S/D.

The VTC curves of our logic inverter are nicely achieved as displayed in Figure 6c. The VTC curves were achieved under low supply voltages (V_{DD}) of –1 V to –7 V, where the maximum voltage gain of ≈5 was obtained at a V_{DD} of –7 V as shown in Figure 6d. We regard that our approach for inverter application is quite simple and practical because the heptazole- and pentacene-channel TFTs have the same S/D electrode which can thus be deposited by single process during inverter fabrication.

3. Conclusions

We have synthesized new indolocarbazole derivative, heptazole, to circumvent the intrinsic problem of existing common organic semiconductors, a marginal band-gap. This new p-type semiconducting heptazole ($C_{26}H_{16}N_2$) could be utilized in the application area of organic electronics, where the photostability is demanded for transparent and wearable electronics. With our heptazole thin-film, optically stable operations could be achieved from organic transistors, since the heptazole OTFT contains a minimal interfacial trap DOS under its high HOMO-LUMO gap of ≈3 eV and shows a moderate field-effect mobility comparable to those of conventional pentacene TFTs, whose active layer has a smaller band gap (1.85 eV) generating large photo-induced current. Benefitting from the photostability and low interfacial trap DOS, our organic image sensor pixel with the heptazole-based OTFTs very well operates coupled with pentacene-based Schottky photodiode. Furthermore, our haptazole thin-film shows almost the similar HOMO level to that of pentacene film, which motivated us toward another heptazole-pentacene coupled device such as a logic inverter using a common S/D electrode, Au. We thus conclude that our small molecule heptazole is quite novel and promising for future organic devices which demand photo-stability and process-simplicity as well.

4. Experimental Section

Synthesis: Heptazole-series bearing pendant N-alkyl chain are reported elsewhere, and synthesis of heptazole bearing nitrogen atom, used in this study, is identical.[6] Unless otherwise stated, reactions were performed under an argon atmosphere using freshly dried solvents. Tetrahydrofuran (THF), dichloromethane, toluene, and ethyl ether were dried by passing them through activated alumina columns. Methanol and benzene were dried over activated molecular sieves and distilled. Degassing was carried out by the standard freeze-pumping-thaw cycle. All other commercially obtained reagents were used as received. All reactions were monitored by thin-layer chromatography using EMD/Merck silica gel 60 F254 pre-coated plates (0.25 mm). The TLC spots were visualized under a UV lamp or using staining solutions such as ceric ammonium molybdate solution, p-anisaldehyde or potassium permanganate solution. Flash column chromatography was performed with the indicated solvents using silica gel (GS60–40/75) purchased from Fuji Silysia Chemical. 1H NMR and 13C spectra were recorded at 400 MHz (Varian Mercury 400 MHz) or 600 MHz (Varian VNMRS 600 MHz). Chemical shifts are reported relative to tetramethylsilane (0 ppm), internal chloroform (1H, δ = 7.26, 13C, δ = 77.1), or DMSO (1H, δ = 2.50, 13C, δ = 39.5). Infrared spectra were recorded on an ABB FTLA2000 FTIR spectrometer. High resolution mass spectra were measured using the FAB method.

Dibenzyl 5,6,13,14-tetrahydrobenzo[a]benzo[6,7]indolo[2,3-h]carbazole-8,16-dicarboxylate 5: To a flask containing acetonitrile (30 mL) and a few drops of conc. H_2SO_4 were added dibenzyl 1,1′-(1,4-phenylene) bis(hydrazinecarboxylate) 3 (500 mg, 1.2 mmol) and α -tetralone 4 (396 mg, 2.7 mmol) at room temperature (RT).[12] The reaction mixture was heated under reflux until all starting material was consumed as judged by TLC. After completion, the reaction mixture was cooled down to RT and filtered off. The solid product collected on a funnel was thoroughly washed by acetonitrile and the combined organic solution was concentrated to give a mixture of 5 and 5' (3:1) in 90% total yield. FT-IR (KBr): 3128, 2312, 1729, 1387, 1222, 1156 cm^{-1}; HRMS (FAB) calculated for $C_{42}H_{32}N_2O_4$ (M^+) 628.2357, found 628.2363.

Dibenzyl benzo[a]benzo[6,7]indolo[2,3-h]carbazole-8,16-dicarboxylate 6: To a suspension of 5 and 5′ (3:1, 597 mg, 0.9 mmol) in benzene (50 mL) was added DDQ (1.22 g, 5.7 mmol) at rt. The resulting mixture was stirred for one day at RT. After the completion of the reaction, the reaction mixture was concentrated in vacuo and added with K_2CO_3 (791 mg, 5.7 mmol), methanol (30 mL) and distilled H_2O (10 mL). The mixture was then heated at 60 °C for 30 min. The reaction mixture was cooled down to RT, filtered off, oven-dried and recrystallized from EtOAc to give 6 as yellow solids. ^{1}H NMR(DMSO-d_6) δ 8.76 (s, 2H), 8.29 (d, J = 8.4 Hz, 2H), 8.06 (dd, J = 8.0, 7.2 Hz, 4H), 7.62 (d, J = 7.2 Hz, 4H), 7.52 (m, 5H), 7.42 (m, 5H), 5.67 (s, 4H); FT-IR (KBr): 3129, 1738, 1400, 1164 cm^{-1}; HRMS (FAB) calculated for $C_{42}H_{28}N_2O_4$ (M^+) 624.2044, found 624.2051.

8,16-Dihydrobenzo[a]benzo[6,7]indolo[2,3-h]carbazole 7: To a suspension of 6 (100 mg, 0.16 mmol) in THF was added 1 m TBAF in tetra-*n*-butylammonium fluoride (TBAF) in THF (0.8 mL, 0.8 mmol) at RT. The reaction mixture was heated under reflux. After 8 h, the reaction mixture was cooled to RT and quenched by adding 1 m aqueous HCl. The resulting yellow slurry was filtered off, washed with EtOAc and distilled H_2O and dried to give 7 (48 mg) in 80% yield. ^{1}H NMR (DMSO-d_6) δ 12.00 (bs, 2H), 8.56 (d, J = 8.0 Hz, 2H), 8.36 (d, J = 8.4 Hz, 2H), 8.32 (s, 2H), 8.04 (d, J = 8.4 Hz, 2H), 7.62 (t, J = 7.4 Hz, 2H), 7.53 (t, J = 7.4 Hz, 2H); ^{13}C NMR (DMSO-d_6) δ 136.6, 134.9, 131.9, 128.5, 125.1, 125.0, 122.9, 122.0, 121.1, 119.7, 118.1, 117.3, 100.2; HRMS (FAB) calculated for $C_{26}H_{16}N_2$ (M^+) 356.1308, found 356.1311.

Thin-Film and Device Characterization: Thin organic film samples were prepared on appropriate substrates for UV-visible absorption (on glass substrate), PL (on Si substrate), ultra-violet photoelectron spectroscopy (UPS on ITO glass), AFM (on CYTOP), and XRD measurements (on Si). All I–V characteristics of the image pixels, TFTs, inverters, and diodes were measured using a semiconductor parameter analyzer (HP 4155C, Agilent Technologies) either in the dark or under light illumination in an air ambient (relative humidity ≈30%). For any white light illumination of the pixel, commercial white-LEDs and LED bundles were used. The optical power of white illuminations were measured using a Si-based optical power meter (TQ8210, ADVANTEST). Photo-excited charge collection spectroscopy (PECCS) was performed with a light source (500 W,

Hg(Xe) arc lamp), a grating monochromator covering the spectral range of 254–1000 nm, and an optical fiber (core diameter of 200 μm) as an optical probe which guide photons onto the channel region of the working device. Photon flux of at least 5×10^{14} cm^{-2} s^{-1} (optical power density, 0.2 mW cm^{-2}) was measured after lights passed through the optical fiber. More details of PECCS theory and experiemental steps are explained elsewhere.[10] All transmittance measurements of the organic thin-films were carried out with a spectrophotometer (Varian Cary 5 G).

Device Fabrication: In order to fabricate an image pixel, a 100 nm-thick Al bottom electrode for heptazole OTFT was thermally evaporated, to be patterned on pre-cleaned glass (Eagle 2000) through one shadow mask. Then, a 50 nm-thin Al_2O_3 film was deposited by atomic layer deposition (ALD) at 200 °C, followed by spin-coating of diluted CYTOP (Ashai glass. Co.) solution on the Al_2O_3 film; the spin-coated CYTOP was post-annealed at 180 °C in ambient oven.[13] Then 60 nm-thin heptazole channel layer (width/length = 500/90 μm) was patterned on the CYTOP/Al_2O_3 double layer by organic molecule beam deposition (OMBD) system as we synthesized and imported the heptazole small-molecule from our co-workers (Luminano Co). Another 100 nm-thick Al electrodes are now patterned on CYTOP by thermal evaporation right below the OTFT area, and then 150 nm-thick pentacene (Aldrich Chem. Co., 99% purity, with no further purification) is deposited on the 100 nm-thick Al anode for Schottky junction formation, followed by semitransparent NiO_x cathode deposition (thermal evaporation) on top. Finally, 200 nm-thick Au source/drain electrodes are patterned on the TFT channel layer by thermal evaporation, to be also connected to Al electrode of Al/pentacene Schottky photodiode. In order to help understanding the pixel processing, we prepared respective image-pixel schemes for the top and cross section views in Figure 4a) and Figure S1 (Supporting Information).The fabrication of an inverter was easier than that of image pixel, since not only an identical gemetry for two OTFTs with different active layers (pentacene and heptazole) was utilized but also the same S/D Au and gate Al electrodes were employed for the two OTFTs which are interconnected in series (see photograph in Figure 6a). The OTFT fabrication method was the same as the one mentioned for pixel transistor.

Supporting Information

Supporting Information is available from the Wiley Online Library or from the author.

Acknowledgements

The authors acknowledge the financial support from NRF (NRL program: Grant No. NRL program, No. 2012-0000126), Brain Korea 21 Program. This work was supported in part by the Yonsei University Research Fund of 2013. The authors express great gratitude to T. W. Ha and Jae. H. Kim at Yonsei University for measuring optical absorption spectra.

Received: May 24, 2013
Revised: July 4, 2013
Published online: September 23, 2013

[1] a) C. C. Dimitrakopoulos, P. R. L. Malenfant, *Adv. Mater.* **2002**, *4*, 99; b) H. Klauk, *Chem. Soc. Rev.* **2010**, *39*, 2643; c) H. Klauk, M. Hali, U. Zschieschang, F. Ede, G. Schmi, C. Dehm, *Appl. Phys. Lett.* **2003**, *82*, 4175; d) D. Kumaki, M. Yahiro, Y. Inoue, S. Tokito, *Appl. Phys. Lett.* **2007**, *90*, 133511; e) S. Lee, B. Koo, J. Shin, E. Lee, H. Park, H. Kim, *Appl. Phys. Lett.* **2006**, *88*, 162109.

[2] a) M. Marchl, M. Edler, A. Haase, A. Fian, G. Trimmel, T. Griesser, B. Stadlober, E. Zojer, *Adv. Mater.* **2010**, *22*, 5361; b) S. H. Kim, H. R. Hwang, H. J. Kwon, J. Jang, *Appl. Phys. Lett.* **2012**, *100*, 053302; c) U. Zschieschang, F. Ante, T. Yamamoto, K. Takimiya, H. Kuwabara, M. Ikeda, T. Sekitani, T. Someya, K. Kern, H. Klauk, *Adv. Mater.* **2010**, *22*, 982; d) K. H. Lee, H. S. Lee, K. Lee, T. Ha, J. H. Kim, S. Im, *Adv. Mater.* **2011**, *23*, 1231; e) H. Klauk, U. Zschieschang, J. Pflaum, M. Halik, *Nature* **2007**, *445*, 745.

[3] a) Y.-Y. Noh, D.-Y. Kim, *Solid State Electron.* **2007**, *51*, 1052; b) H. Klauk, U. Zschieschang, R. T. Weitz, H. Meng, F. Sun, G. Nunes, D. E. Keys, C. R. Fincher, Z. Xiang, *Adv. Mater.* **2007**, *19*, 3882; c) J. Lee, S. S. Kim, K. Kim, J. H. Kim, S. Im, *Appl. Phys. Lett.* **2004**, *84*, 1701; d) K. Lee, M. S. Oh, S. Mun, K. H. Lee, T. W. Ha, J. H. Kim, S. H. K. Park, C. S. Hwang, B. H. Lee, M. M. Sung, S. Im, *Adv. Mater.* **2010**, *22*, 3260.

[4] a) Y. Wu, Y. Li, S. Gardner, B. S. Ong, *J. Am. Chem. Soc.* **2005**, *127*, 614; b) T. Yamamoto, K. Takimiya, *J. Am. Chem. Soc.* **2007**, *129*, 2224; c) H. Ebata, T. Izawa, E. Miyazaki, K. Takimiya, M. Ikeda, H. Kuwabara, T. Yui, *J. Am. Chem. Soc.* **2007**, *129*, 15732.

[5] a) D. Knipp, R. A. Street, A. Völkel, J. Ho, *J. Appl. Phys.* **2003**, *93*, 347; b) D. K. Hwang, C. S. Kim, J.-M. Choi, K. Lee, J. H. Park, E. Kim, H. K. Baik, J. H. Kim, S. Im, *Adv. Mater.* **2006**, *18*, 2299.

[6] a) S. H. Han, C.-G. Cho, US Pat., 0253944 A1, **2011**; b) C.-G. Cho, S. H. Han, Korean Patent application 10-2011-0094493A; c) K. S. Park, S. M. Salunkhe, I. Lim, C.-G. Cho, S.-H. Han, M. M. Sung, *Adv. Mater.* **2013**, *25*, 3351.

[7] a) D. K. Hwang, C. S. Kim, J.-M. Choi, K. Lee, J. H. Park, E. Kim, H. K. Baik, J. H. Kim, S. Im, *Adv. Mater.* **2006**, *18*, 2299; b) H. S. Lee, K. H. Lee, C. H. Park, P. J. Jeon, K. Choi, D.-H. Kim, H.-R. Kim, G.-H. Lee, J. H. Kim, S. Im, *J. Mater. Chem.* **2012**, *22*, 4444.

[8] Y. Lee, H. Lee, S. Park, Y. Yi, *Appl. Phys. Lett.* **2012**, *101*, 233305.

[9] a) N. J. Watkins, Y. Gao, *J. Appl. Phys.* **2003**, *94*, 5782; b) B. G. Streetman, S. Banerjee, *Solid State Electronics Devices*, 5th ed. Prentice Hall, Upper Saddle River, New Jersey **2000**, Ch. 3.

[10] a) K. Lee, M. S. Oh, S. Mun, K. H. Lee, T. W. Ha, J. H. Kim, S. H. K. Park, C. S. Hwang, B. H. Lee, M. M. Sung, S. Im, *Adv. Mater.* **2010**, *22*, 3260; b) J. Lee, B.-L. Lee, J. H. Kim, S. Lee, S. Im, *Phy. Rev. B* **2012**, *85*, 045206; c) K. Lee, B. H. Lee, K. H. Lee, J. H. Park, M. M. Sung, S. Im, *J. Mater. Chem.* **2010**, *20*, 2659.

[11] H. S. Lee, C. H. Park, K. H. Lee, D.-H. Kim, H.-R. Kim, G.-H. Lee, S. Im, *Phys. Status Solidi RRL* **2011**, *5*, 211.

[12] For the synthesis of dibenzyl 1,1′-(1,4-phenylene)bis(hydrazinecarboxylate) **3**, see: I.-K. Park, S.-E. Park, B.-Y. Lim, C.-G. Cho, *Org. Lett.* **2009**, *11*, 5454.

[13] J. H. Park, H. S. Lee, J. Lee, K. Lee, G. Lee, K. H. Yoon, M. M. Sung, S. Im, *Phys. Chem. Chem. Phys.* **2012**, *14*, 14202.